THE NATURE OF THE UV/X-RAY ABSORBER IN PG 2302+029

BASSEM M. SABRA & FRED HAMANN
Department of Astronomy, University of Florida, Gainesville, FL 32611
BUELL T. JANNUZI
National Optical Astronomy Observatory, 950 North Cherry Ave., Tuscon, AZ 85719
IAN M. GEORGE
Joint Center for Astrophysics, Department of Physics, University of Maryland, Baltimore County, 1000 Hilltop Circle, Baltimore, MD 21250
Laboratory for High Energy Astrophysics, Code 662, NASA/Goddard Space Flight Center, Greenbelt, MD 20771
JOSEPH C. SHIELDS
Department of Physics & Astronomy, Ohio University, Athens, OH 45701

Draft version February 3, 2003

ABSTRACT

We present *Chandra* X-ray observations of the radio-quiet QSO PG 2302+029. This quasar has a rare system of ultra-high velocity ($-56,000$ km s^{-1}) UV absorption lines that form in an outflow from the active nucleus (Jannuzi et al. 2003). The *Chandra* data indicate that soft X-ray absorption is also present. We perform a joint UV and X-ray analysis, using photoionization calculations, to detemine the nature of the absorbing gas. The UV and X-ray datasets were not obtained simultaneously. Nonetheless, our analysis suggests that the X-ray absorption occurs at high velocities in the same general region as the UV absorber. There are not enough constraints to rule out multi-zone models. In fact, the distinct broad and narrow UV line profiles clearly indicate that multiple zones are present. Our preferred estimates of the ionization and total column density in the X-ray absorber ($\log U = 1.6$, $N_{\rm H} = 10^{22.4}$ cm^{-2}) over predict the O VI $\lambda\lambda$1032, 1038 absorption *unless* the X-ray absorber is also outflowing at $\sim 56,000$ km s^{-1}, but they over predict the Ne VIII $\lambda\lambda$770, 780 absorption at *all* velocities. If we assume that the X-ray absorbing gas is outflowing at the same velocity of the UV-absorbing wind and that the wind is radiatively accelerated, then the outflow must be launched at a radius of $\leq 10^{15}$ cm from the central continuum source. The smallness of this radius casts doubts on the assumption of radiative acceleration.

Subject headings: galaxies: active—quasars: absorption lines—quasars: individual (PG 2302+029)—X-rays: galaxies

1. INTRODUCTION

X-ray absorption in quasars provides a powerful tool to study QSO environments. The signatures of this absorption are typically the suppression of soft X-rays and /or the presence of absorption edges from O VII and O VIII near 0.8 keV (Reynolds 1997; George et al. 1998). The strength of these features depends mainly on the degree of ionization and total column density. The relationship of the X-ray absorber to other components of the quasar environs, especially the UV absorbing gas, is not well understood. A natural question is whether these features originate in the same gas.

The best-known intrinsic UV absorption lines in QSOs are the broad absorption lines (BALs), but recent work has shown that some of the observed narrow absorption lines (NALs) and "mini-BALs" are also intrinsic to QSO environments (Barlow, Hamann & Sargent 1997; Hamann et al. 1997a and 1997b). These features can have velocity shifts comparable to the BALs (up to $-51,000$ km s^{-1} in one confirmed case; Hamann et al. 1997b) but the narrow line widths (from <100 km s^{-1} to a few thousand km s^{-1}) require outflows with much smaller line-of-sight velocity dispersions. BALs, mini-BALs, and intrinsic NALs are each rare in QSO spectra, but the outflows that cause them might be common if, as expected, the gas covers a small fraction of the sky as seen from the central source. Among Seyfert 1 galaxies, 50% show intrinsic UV absorption (Crenshaw et al. 1999), and there is also a one-to-one correlation between the detection of X-ray absorption in Seyfert 1 galaxies and the appearance of intrinsic UV absorption lines (Crenshaw et al. 1999).

In QSOs, X-ray absorption is much rarer (Laor et al. 1997). Brandt, Laor, & Wills (2000) showed that QSOs with BALs are all significantly weaker soft X-ray sources than comparable-luminosity QSOs without BALs. Positive X-ray detections of BALQSOs (e.g., Mathur, Elvis, & Singh 1995; Green et al. 2001; Sabra & Hamann 2001; Gallagher et al. 2002) reveal large absorbing columns of $N_{\rm H} \gtrsim 10^{23}$ cm^{-2}. QSOs with weaker intrinsic UV absorption lines, e.g., the NALs and mini-BALs, appear to have systematically weaker X-ray absorption (Brandt et al. 2000). However, more work is needed to characterize the X-ray absorption in quasars with different types/strengths of UV absorption. Studies of X-ray absorbers in quasars, especially in relation to the UV absorption lines, will have profound impact on our knowledge of quasar wind properties, such as the acceleration mechanism, outflow geometry, wind launch radius, and mass loss rate (e.g., Mathur et al. 1995; Murray, Chiang, & Grossman 1995; Hamann 1998; Sabra & Hamann 2001). For example, it is difficult to radiatively accelerate an outflow with a large column

density, unless it is launched from the inner most regions of the accretion disk.

In this paper we will discuss *Chandra* X-ray observations of the QSO PG 2302+029. This object shows a system of intrinsic UV absorption lines that have a velocity shift of $-56,000$ km s^{-1} (Jannuzi et al. 1996) with respect to the systemic velocity of the QSO ($z_{ems} = 1.044$). The system consists of NALs ($FWHM \approx 330$ km s^{-1}) at $z = 0.7016$ and a "mini-BAL" system ($FWHM \approx 3300$ km s^{-1}) at $z = 0.695$ (Jannuzi et al. 1996; 1998). It is also characterized by being an X-ray faint source with an *HEAO-1* A-2 flux upper limit at 2 keV of 4×10^{-12} erg s^{-1} cm^{-2} (Della Ceca et al. 1990). Our aim is to determine the properties of the X-ray spectrum, search for signs of absorption, and define the relationship between the UV and X-ray absorbing gas. We also discuss the location of the absorber, and the potential implications of high-velocity X-ray absorption for the wind dynamics. If the X-ray and UV absorbers are the same, then the $-56,000$ km s^{-1} velocity shift of the UV absorption lines in PG 2302+029 is potentially resolvable with the Advanced Imaging Spectrometer (ACIS), given sharp features and adequate signal-to-noise ratio.

2. OBSERVATIONS AND DATA REDUCTION

We observed PG 2302+029 with *Chandra* using ACIS on 7 January 2000. We used the most recent (2 November 2000) re-processed data released by the Chandra X-ray Center for our analysis. No filtering for high background or bad aspect times was required because the light curves did not show any flare-ups in the count rate and the aspect solution, the pattern by which the telescope was dithered to distribute the incoming photons over different pixels to minimize pixel-to-pixel variation, did not have any outlying points. We performed data extraction and calibration using version 1.4 of the Chandra Interactive Analysis of Observations (CIAO). We created the response matrix and ancillary response files using calibration data provided when the chip temperature during observations was $-120°$ C.

We extracted the source counts from a circular region of radius of 5″ while the background region was an annulus with radii between 10″ and 20″, both centered on the position of PG 2302+029. The position of PG 2302+029 (α(J2000) = $23^h04^m44^s$, δ(J2000) = $+03°11'46''$), as determined from the ACIS image, coincides to within $\sim 1''$ with the optical position of the source reported in Schneider et al. (1992). We obtained a total of 391 ± 21 counts in an exposure time of 48 ksec across the observed energy range $\sim 0.4 - 4.0$ keV.

3. ANALYSIS AND RESULTS

We bin the spectrum to have at least 30 counts/bin and use XSPEC (Arnaud 1996) to perform the analysis. The low count rate indicates that X-ray absorption may be present. We, therefore, consider fits to the data that include an X-ray continuum attentuated through an ionized X-ray absorber. Neutral X-ray absorption can be ruled out because the UV spectra do not contain any low-ionization metal lines that can be identified with the NAL and/or mini-BAL systems discussed in this paper (Jannuzi et al. 1996; Jannuzi et al. 2003). We model the ionized absorbers using the photoionization code CLOUDY (Ferland et al. 1998) assuming solar abundances.

We use this code to generate grids of absorbed continua in the following way: The incident continuum is a piecewise powerlaw, $f_\nu \propto \nu^{-\alpha}$, (Zheng et al. 1997; Laor et al. 1997; Telfer et al. 2002) and is displayed in Figure 1. The far-UV part of the spectrum is characterized by the 2-point spectral index α_{ox}, which relates the flux densities at 2500 Å and 2 keV: $\alpha_{ox} = 0.384 \log(f_\nu(2500Å)/f_\nu(2\mathrm{keV}))$. We use the B magnitude of 16.3 for PG 2302+029 to anchor the spectral energy distribution (SED) at 2500Å, taking into account the appropriate $k-$correction (Green 1996). Consequently, the X-ray flux density is specified through α_{ox}. We step α_{ox} from 1.6 to 2.2 in increments of 0.2. This effectively gives us 4 different unabsorbed spectra representing 4 possible intrinsic SEDs from the quasar's central engine, leading to 4 different intrinsic X-ray luminosities (cf. Figure 1). Each SED is then attenuated through an ionized absorber. The amount of absorption largely depends on the intrinsic total hydrogen column density, $N_{\rm H}$ (cm^{-2}), and the ionization parameter, U, defined as the ratio of the density of hydrogen ionizing photons to that of hydrogen particles ($H^0 + H^+$). For each of our 4 SEDs, we create a grid of attenuated continua by calculating ionized absorbers on a grid of U and $N_{\rm H}$. Therefore, for every SED, there will be a grid of absorbed X-ray spectra identified by the (U, $N_{\rm H}$) combinations of the absorber through which they were transmitted.

XSPEC incorporates a χ^2 minimization scheme that allows us to find the best fitting attenuated continuum to the X-ray spectrum of PG 2302+029. We note that all our X-ray fits include attenuation by a Galactic column density of $N_{\rm H}^{Gal.} = 5 \times 10^{20}$ cm^{-2} (Lockman & Savage 1995) and the presence of an emission line with a Gaussian profile at ~ 3 keV (probably Fe Kα at the redshift of the QSO). The significance of the Fe Kα detection is clearly very low, given just 391 counts (see Figure 2), but we include it in our fits because the line is plausibly present and it improves the χ^2 results. We adjust the properties of the best Fe Kα fit— normalization (1.7×10^{-6} photon s^{-1} cm^{-2} keV^{-1}), width (0.3 keV), and energy (2.9 keV)— by hand after finding the best fit for the continuum in other parts of the spectrum. Our scheme also allows us to place the intrinsic absorber at any redshift we want. Naturally, we choose to place it either at the systemic redshift of the QSO, $z_{XAbs} = z_{QSO} \approx 1$, or at the redshift of the UV absorption lines, $z_{Xabs} = z_{UVabs} \approx 0.7$.

For a specific absorber redshift and for each of our 4 grids corresponding to the 4 intrinsic SEDs, we fit the data, with U and $N_{\rm H}$ as free parameters, and note the value of the lowest reduced χ^2, χ^2_ν, possible for that particular SED, and hence α_{ox}, and z. Upon comparison between the 8 χ^2_ν values, we find that the lowest $\chi^2_\nu \approx 1$, was that for the SED with intrinsic $\alpha_{ox} = 2.0$, corresponding to a far-UV/X-ray slope of $\alpha_{\rm EUV} = 2.4$, for both $z = 0.7$ and 1.0. The rest of the SEDs are rejected at the 95% confidence level, regardless of the amount of intrinsic absorption.

The need for intrinsic absorption is illustrated in Figure 2, where we show the X-ray spectrum of PG 2302+029 together with best possible fits, for the continuum with $\alpha_{ox} = 2.0$, with no intrinsic absorption (upper panel), and with an ionized absorber at $z = 0.7$ (lower panel). Clearly,

the fit that includes intrinsic ionized absorption is much better than the one that does not. In particular, the unabsorbed spectrum fits the data well at high energies, but it substantially over predicts the counts in soft X-rays. An X-ray absorber naturally lowers the soft X-ray flux to the measured values.

Figure 3 shows overplots of the 67%, 90%, and 99% confidence contours from fitting the data for the case where the X-ray absorber is at the emission redshift, $z_{XAbs} = z_{QSO}$ (solid contours), and where the X-ray absorber matches the UV absorber redshift, $z_{XAbs} = z_{UVabs}$ (dotted contours). For the $z_{XAbs} = z_{QSO}$ case we find that $N_{\rm H} = 10^{22.8\pm0.2}$ cm^{-2} and $\log U = 2.2^{+0.1}_{-0.2}$ while for the $z_{XAbs} = z_{UVabs}$, $N_{\rm H} = 10^{22.4\pm0.1}$ cm^{-2} and $\log U = 1.6 \pm 0.3$, where all errors are at the 90% confidence level. The χ^2_ν in both cases is ~ 1, and therefore the fits do not constrain the redshift of thte X-ray absorber. Note that these results were derived assuming a fixed X-ray powerlaw index of $\alpha_x = 0.9$. We did not explore other X-ray spectral slopes because the data quality is not sufficient to constrain additional free parameters.

4. DISCUSSION

4.1. *Intrinsic X-ray Brightness*

Our finding in Section 3 that the intrinsic $\alpha_{\rm ox}$ is 2.0 for PG 2302+029 deserves more attention. It has been known that there is a correlation between the optical luminosity at 2500Å of a quasar and its intrinsic $\alpha_{\rm ox}$ (e.g., Yuan et al. 1998 and references therein). The relation shows a wide scatter in the distribution. The average $\alpha_{\rm ox}$ for radio quiet QSOs, such as PG 2302+029 (Kellerman et al. 1989), is 1.7 (Yuan et al. 1998; Vignali, Brandt, & Schneider 2003). PG 2302+029, with $\alpha_{\rm ox} = 2.0$ and $L_\nu(2500Å) \approx 10^{31.8}$ erg s^{-1} Hz^{-1}, is still consistent with the scatter in the $L_\nu - \alpha_{\rm ox}$ distribution discussed in Yuan et al. (1998), although it is $\sim 10^{\frac{2.0-1.7}{0.384}} \sim 6$ times fainter at 2 keV, in the rest frame, than a quasar with comparable UV luminosity. This faintness is probably due to X-ray absorption.

4.2. *The UV/X-ray Relationship*

We perform a joint analysis of the our X-ray spectra and previous HST UV data (Jannuzi et al. 1996; Jannuzi et al. 1998; Jannuzi et al. 2003) to explore the relationship between the UV and X-ray absorbers. The HST data taken over two epochs (UT dates 19 May 1994 and 21, 24 December 1998) reveal variability in the strength of the UV absorption lines (Jannuzi 2002). These results confirm the intrinsic nature of the UV absorption, but it is important to keep in mind that the X-ray observations are not simulateneous with the HST dataset.

The 1994 Faint Object Spectrograph (FOS) spectra show marginally resolved narrow absorption lines (NALs, $FWHM \approx 330$ km s^{-1}, compared to a resolution of ≈ 270 km s^{-1}) of O VI $\lambda\lambda$1032, 1038, Lyα, N V $\lambda\lambda$1239, 1243, and C IV $\lambda\lambda$1548, 1551 at $z_{abs}^{narrow} = 0.7016$; broad absorption features (mini-BALs, $FWHM \approx 3300$ km s^{-1}) from O VI, N V, C IV are seen at $z_{abs}^{broad} = 0.695$ (Jannuzi et al. 1996). Space Telescope Imaging Spectrograph (STIS) data from 1998 reveal that the absorption, mini-BALs and NALs, in O VI and N V dramatically weakened to become unmeasurable, while the mini-BALs of C IV also diminished in strength (Jannuzi 2002; Jannuzi et al. 2003). The STIS spectra were obtained using the G140L and G230LB gratings, providing coverage from 1200 to 3000 Å at a spectral resolution of roughly R=500, or approximately a factor of two lower than the earlier FOS spectra. For further comparison of the STIS and FOS spectra, Jannuzi et al. (2003) convolved the FOS spectra to match the lower resolution of the STIS data. The observed absorption systems were then fit with Gaussians to determine the equivalent widths and line widths for each feature. These measurements were used, as detailed below, to constrain the column densities listed in Table 1.

From the standpoint of our analysis we are dealing effectively with 4 UV absorbers and 1 X-ray absorber: the broad and narrow-line UV absorbers of the 1994 epoch, the broad and narrow-line UV absorbers of 1998, and the X-ray absorber of 2000. We compare the properties of all these absorbers to investigate the UV/X-ray relationship.

We present in Figure 4 contours (solid lines) of ionic column densities of C IV, N V, O VI, and H I generated by photoionization calculations, using the $\alpha_{\rm ox} = 2.0$ SED from section 3, on a grid of the ionization parameter and the total hydrogen column density, assuming solar abundances. The closed contours in Figure 4 are the 90% confidence contours calculated from the X-ray data (cf. Figure 3). The solid-line, closed contour is for the X-ray absorber at the redshift of the PG 2302+029, while the dotted-line one is for the X-ray absorber at the redshift of the UV absorber. The long-dashed and short-dashed contours denote the values of the ionic column densities from the broad lines and narrow lines, respectively, in the FOS spectra (see Jannuzi et al. 1996; 2003 for a detailed discussion of the UV data themselves). We do not show contours for the N V NALs since the 1239 Å line appears to be weaker than the 1243 Å line, probably due to the low signal-to-noise ratio, contrary to atomic physics.

We calculated UV the ionic column densities through a curve-of-growth analysis (Spitzer 1978) using the equivalent widths and FWHMs (to estimate the Doppler b parameters) reported in Jannuzi et al. (2003), under the assumption of homogenous complete coverage by the absorber of the continuum source. The results are listed in Table 1. The Doppler b parameter is a convenient way of characterizing the line-of-sight velocity field; we do not imply that thermal broadening is the cause of the line width. We include only the lines measured directly by Jannuzi et al. (2003). We do not list upper limits. The only mini-BALs and NALs in the STIS data that are discernable are those of C IV (see Table 1). We do not show their contours in Figure 4 to avoid cluttering the plots. We assume that the unresolved STIS NALs have the same line widths as their marginally resolved FOS counterparts.

We wish to make three comments here about the UV measurements. First, the C IV NAL doublets have equivalent width ratios somewhere between the optically thin, 2:1, and the optically thick, 1:1, limits. We therefore expect that these lines are not dominated by unresolved optically thick components, and our simple curve-of-growth analysis should yield reasonably accurate column densities that are, in any case, firm lower limits. Second, the mini-BALs are in fact blended doublets, implying that we have no contraints on partial coverage and our derived column densities for these lines are merely lower limits. Finally,

given an equivalent width, we calculated the resulting ionic column density, the one shown in Figure 4. We assumed that the mini-BAL is due to a single transition. The oscillator strength of this transition is the sum of the two oscillator strengths of the doublet. The rest wavelength of the single transition is the oscillator-strength-weighted average of the rest wavelengths of the doublet lines. A more appropriate method would be to use the prescription presented in Junkkarinen, Burbidge, & Smith (1983) where an effective optical depth is calculated at every point across the line profile taking into account the combined contributions of the lines in the doublet. Upon experimentation with the STIS C IV mini-BALs, we found that the difference between the two methods is $\sim 30\%$, within the measurements errors involved and making minimal difference in Figure 4.

While weak low-ionization UV absorption lines are seen at the redshift of the quasar and may be of a different nature than the NALs and mini-BALs we are discussing here (Jannuzi et al. 1998), high-ionization UV absorption lines are absent at this redshift. Moreover, there is no Lyman break, at any redshift, in the UV spectrum, and hence the total hydrogen column density in a low-ionization/neutral absorbing component is not high enough to lead to any observable effects on the X-ray spectrum. Our best fit to the X-ray absorber at $z_{Xabs} = z_{QSO}$ over predicts the OVI line absorption at this redshift. In particular, the predicted OVI column density at this redshift, $10^{15.6}$ cm^{-2}, would lead to an equivalent width of ~ 9 Å and ~ 3 Å in the observed frame if the lines have a Doppler parameter of $b \approx 2000$ km s^{-1} and $b \approx 200$ km s^{-1}, like the high-velocity mini-BALs and NALs, respectively. These features should be detectable at $\gtrsim 7\sigma$ in the FOS and STIS spectra. Their absence suggests that the X-ray absorber is *not* at the quasar systemic velocity. Note that these results do not depend on our assumption of solar metallicity, as long as the relative metal abundances are roughly in their solar ratios. The X-ray absorption is dominated by metal ions, and we use our fits to that to predict the strength of the metal lines in the UV. The relative abundance of hydrogen, therefore, is not a significant factor.

Another important constraint on the UV – X-ray relationship comes from the Ne VIII column densities (Figure 5). The Ne VIII lines are at 770 and 780 Å, within the spectral coverage of the STIS observations but not the FOS. The fact that they are high-ionization lines implies that they are good tracers of the X-ray gas. Our best fits to the X-ray data predict Ne VIII column densities of $\sim 10^{16.5}$ cm^{-2} if $z_{Xabs} = z_{QSO}$ and $\sim 10^{17.2}$ cm^{-2} if $z_{Xabs} = z_{UVabs}$. For Doppler parameters appropriate for the mini-BALs or NALs, $b \approx 2000$ km s^{-1} or $b \approx 200$ km s^{-1}, respectively, we find that the Ne VIII column densities predicted by the X-rays should produce easily measurable UV lines ($\gtrsim 40\sigma$), corresponding to observed frame equivalent widths of ~ 40 Å or ~ 3 Å respectively. However, there is no Ne VIII absorption detected at either redshift.

There are several possible explanations for the apparent discrepancies. First, the absorber overall is complex and time variable. The complexity is evident from the distinct UV kinematic components, e.g., the NALs and mini-BALs. Also, the column densities derived from the UV lines do not define an isolated location in the $\log U$ versus $\log N_H$ plane (Fig.4), suggesting that the NAL and mini-BAL regions both have multiple zones (with different values of U and N_H). Third, as we have noted above, the NALs and mini-BALs both varied between the 1994 and 1998 HST observations (Jannuzi 2002), and neither of those measurements was simultaneous with the X-ray data obtained in 2000. Finally, the true uncertainties in U and $N_{\rm H}$ of the X-ray absorber are likely to be larger than shown in Figure 3. Those results are based on fits that fixed the underlying continuum shape. Letting both the continuum shape and absorber properties vary in the fit would clearly lead to more uncertain results – although, without pursuing that option, it is not clear if the the predicted Ne VIII absorption could be as low as the upper limit from the UV spectrum.

Another complication is that the UV lines may be affected by partial coverage. If the absorbing gas does not fully cover the background light source, as we have assumed above, then there can be unabsorbed light filling in the bottoms of the UV line troughs and the column densities inferred from the lines will be only lower limits. Studies of other sources show that the coverage fraction can differ between ions and vary with velocity (across the line profiles) in the same ion (Hamann et al. 1997, Barlow & Sargent 1997, Barlow, Sargent & Hamann 1997). Our column density estimates all assume 100% coverage. We can determine from the doublet ratios of the NALs that those lines are not optically thick absorption masked by partial coverage, i.e., their derived column densities should be reasonable (section 4.2). Moreover, we have no diagnostic of partial coverage for the mini-BALs. We must therefore keep in mind that their derived column densities are, strictly speaking, only lower limits. Similarily, the line strengths predicted from the X-ray column densities, e.g. for O VI and Ne VIII above, are lower limits because of the assumption of 100% coverage in the X-ray fits.

In summary, the strengths of most of the UV lines are consistent with the X-ray measurements, if the X-ray and UV absorbers are outflowing at the same speed. The absence of high-ionization absorption lines at the quasar's redshift argues for the UV and X-ray absorbers occuring in the same general region at high velocity. However, the X-ray observations overpredict the *high-ionization* UV lines of Ne VIII at all velocities. Simultaneous UV and X-ray observations are needed to probe the UV – X-ray relationship further.

4.3. *Wind Dynamics*

If we assume the X-ray absorbing gas is outflowing with the UV absorber, then we can use the outflow velocity determined from the UV lines together with the X-ray measured total hydrogen column density to test the viability of radiative acceleration of the wind. Hamann (1998) found that the terminal velocity ($v_{terminal}$) of a radiatively accelerated wind is related (cf. equation 3 of Hamann 1998) to the total luminosity of the quasar, the mass of its central blackhole, the total column density of the wind ($N_{\rm H}$), the radius at which it is launched (R_{launch}), and the fraction (f_L) of incident continuum energy absorbed or scattered by the wind along an average line of sight.

For BALs, Hamann (1998) estimated that f_L could be on the order of a few tenths. However, the narrower and shallower lines in PG 2302+029 will intercept less con-

tinuum flux. Moreover, lower column densities compared to BAL flows imply that reprocessing overall is less efficient. We, therefore, assume that $f_L \leq 0.1$ for our present analysis. We also adopt representative values of the blackhole mass, 10^8 $M_\odot$, and luminosity, 10^{46} erg s^{-1}, which is the Eddington luminosity associated with that mass. We assume that $v_{terminal} = 56,000$ km s^{-1} and $N_H = 2.34 \times 10^{22}$ cm^{-2}. These values are the outflow velocity of the UV lines (Jannuzi et al. 1996) and the column density we determined from the X-rays if the absorber is at $z = 0.7$ (see end of section 3). Substituting all these numbers into equation (3) of Hamann (1998), we find that the launch radius is $\leq 10^{15}$ cm ≈ 100 $R_{Schwarzchild}$. Therefore, if the wind is radiatively accelerated, it must be launched very near to the black hole.

The mass loss rate implied by this radius is $\leq 0.1\ Q\ M_\odot$ yr^{-1}, where Q is the global covering factor $\Omega/4\pi$ (Hamann & Brandt 2002, in preparation). The density of the flow at this launch radius should be $n_H \gtrsim 10^{11}$ cm^{-3}, if it is photoionized with $\log U = 1.6$ appropriate for the X-ray absorber (see Hamann & Brandt 2002 for explicit equations).

4.4. *Geometry and Physical Models*

The small launch radius required for a high-velocity X-ray absorber may be problematic for models of the outflow in PG 2302+029. For comparison, this maximum launch radius is *much* smaller than the nominal radius of the broad emission line region for a quasar of the same luminosity ($R_{BLR} \approx 2 \times 10^{18}$ cm, based on reverberation studies, e.g., Kaspi et al. 2000). On the other hand, the size of the X-ray continuum source is $\sim 10^{14}$ cm (e.g., Peterson 1993), an order of magnitude smaller than the launch radius derived above. Given the small launch radius, it seems likely that the X-ray absorber is either *not* radiatively accelerated, or *not* outflowing at the same high speed as the UV lines.

In either case, the absence of high-ionization UV absorption near the systemic velocity places another important constraint on wind models. If it is a steady- state flow, then the acceleration must occur in a region that does not intersect our sightline to the continuum source. Models of outflows that lead to such UV lines have been discussed by Murray et al. (1995), Murray & Chiang (1995), and Elvis (2000). In these scenarios, the wind is initially perpendicular to the accretion disk. As it flows farther from the disk, the radiation pressure accelerating it bends and flares in the radial direction. Oblique lines of sight then could pass through the bent part of the wind, thus explaining the absence of zero-velocity absorption.

The models mentioned in the previous paragraph differ in subtle ways. Murray et al. (1995) described a case in which the X-ray absorber is at rest. Its function is to shield the UV gas from soft X-rays and prevent it from becoming highly ionized, in which case resonant line driving would not be effective. Another variant of this scheme is the possibility of a self-shielding wind (Murray & Chiang 1995; Elvis 2000). The X-ray and UV absorption arise in the same outflowing gas. The high column density of the wind requires a small launch radius, although probably larger than the radius we derive in section 4.3.

5. CONCLUSIONS

We presented *Chandra* X-ray observations of the radio-quiet QSO PG 2302+029 and demonstrated the presence of soft X-ray absorption in its spectrum. Older UV spectra of this quasar have been used to identify the presence of rarely observed ultra-high velocity ($-56,000$ km s^{-1}) absorption lines consistent with this quasar containing a remarkable outflow from its active nucleus (Jannuzi et al. 1996, Jannuzi et al. 2003). Using photoionization models and the combined X-ray and UV data sets we have investigated the possible physical properties of the gas producing the X-ray and UV absorption. We suggest that the X-ray absorption also occurs at high velocities in the same general region as the UV absorber. There are not enough constraints to rule out multi-zone models. Multi-zone models are required if the distinct broad and narrow UV line profiles are both intrinsic to the QSO. The properties of the X-ray and UV absorption, as inferred from the data, are consistent with each other, if the X-ray absorbing gas is outflowing with the UV absorber. However, the X-ray data over predict the strength of the high-ionization UV lines of Ne VIII at all velocities. If we assume the X-ray absorbing gas is in an outflow with the same velocity as the gas producing the UV-absorbing wind and that such winds are radiatively accelerated, then the outflow must be started at a radius of $\leq 10^{15}$ cm from the central source of the radiation.

Acknowledgements: We wish to acknowledge support through *Chandra* grants GO 0-1123X and GO 0-1157X. BTJ acknowledges support from the National Science Foundation through their support of the National Optical Astronomy Observatory, which is operated by the Association of Universities for Research in Astronomy, Inc. (A.U.R.A.) under cooperative agreement with the National Science Foundation and from NASA through a grant to proposal GO-07348.01-A from the Space Telescope Science Institute, which is operated by A.U.R.A., Inc., under NASA contract NAS5-26555

REFERENCES

Arnaud, K. A. 1996, Astronomical Data Analysis Software and Systems V, eds. Jacoby G. and Barnes J., p17, ASP Conf. Series volume 101
Barlow, T. A., & Sargent, W. L. W. 1997, AJ, 113, 136
Barlow, T. A., Hamann, F., & Sargent, W. L. W. 1997, ASP Conf. Ser., 128, 13
Brandt, W. N., Laor, A., & Wills, B. J. 2000, ApJ, 528, 637
Crenshaw, D. M., Kraemer, S. B., Boggess, A., Maran, S. P., Mushotzky, R. F., & Wu, Chi-Chao 1999, ApJ, 516, 750
Della Ceca, R. Palumbo, G. G. C., Peris, M., Boldt, E. A., Marshall, E. E., & de Zotti, G. 1990, ApJS, 72, 47
Elvis, M. 2000, ApJ, 545, 63
Ferland, G., Korista, K. T., Verner, D. A., Ferguson, J. W., Kingdon, J. B., & Verner, E. M. 1998, PASP, 110, 761
Gallagher, S. C., Brandt, W. N., Chartas, G., & Garmire, G. P. 2002, ApJ, 567, 37
George, I. A., Turner, T. J., Netzer, H., Nandra, K., Mushotzky, R. F., & Yaqoob, T. 1998, ApJS, 114, 73
Green, P. J. 1996, ApJ, 467, 61
Green, P. J., Aldcroft, T. L., Mathur, S., Wilkes, B. J, & Elvis, M. 2001, ApJ, 558, 109
Hamann, F. 1997, ApJS, 109, 279
Hamann, F., et al. 1997a, ApJ, 478, 80
Hamann, F., et al. 1997b, ASP Conf. Ser., 128, 19
Hamann, F. 1998, ApJ, 500, 798

Hamann, F., & Brandt, W. N. 2002, in prep.
Jannuzi, B., T., et al. 1996, ApJ, 470, 11
Jannuzi, B., T., et al. 1998, ApJS, 118, 1
Jannuzi, B., T. 2002, in Extragalactic Gas at Low Redshift, eds. Mulchey J. S. and Stocke J. T., p13, ASP Conf. Series volume 254
Jannuzi, B., T., et al. 2003, in prep.
Junkkarinen, V. T., Burbidge, E. M., & Smith, H. E. 1983, ApJ, 265, 51
Kellerman, K. I., Sramek, R., Schmidt, M., Shaffer, D. B., & Green, R. 1989, AJ, 98, 1195
Kaspi, S., Smith, P. S., Netzer, H., Maoz, D., Jannuzi, B. T., & Giveon, U. 2000, ApJ, 533, 631
Laor, A., Fiore, F., Elvis, M., Wilkes, B. J., & McDowell, J. C. 1997, ApJ, 477, 93
Lockman, F. J., & Savage, B. D. 1995, ApJS, 97, 1
Mathur, S., Elvis, M., & Singh, K. 1995, ApJ, 455, L9
Murray, N., & Chiang, J. 1995, ApJ, 454, L101
Murray, N., Chiang, J., Grossman, J. A., & Voit, G. M. 1995, ApJ, 451, L498
Peterson, B .M. 1997, An Introduction to Active Galactic Nuclei (Cambridge: Cambridge University Press)
Reynolds, C. S. 1997, MNRAS, 286, 513
Sabra, B. M., & Hamann, F. 2001, ApJ, 563, 555
Schneider, D. P., et al. 1992, PASP, 104, 678
Spitzer, L., Jr. 1978, Physical Processes in the Interstellar Medium (New York: Wiley)
Telfer, Zheng, W., Kriss, G., & Davidsen, A. F. 2002, ApJ, 565, 773
Vignali, C., Brandt, W. N., & Schneider, D. P. 2003, AJ, 125, 433
Yuan, W., Siebert, J., & Brinkmann, W., 1998, A&A, 334, 498
Zheng, W., Kriss, G. A., Telfer, R. C., Grimes, J. P., & Davidsen, A. F. 1997, ApJ, 475, 469

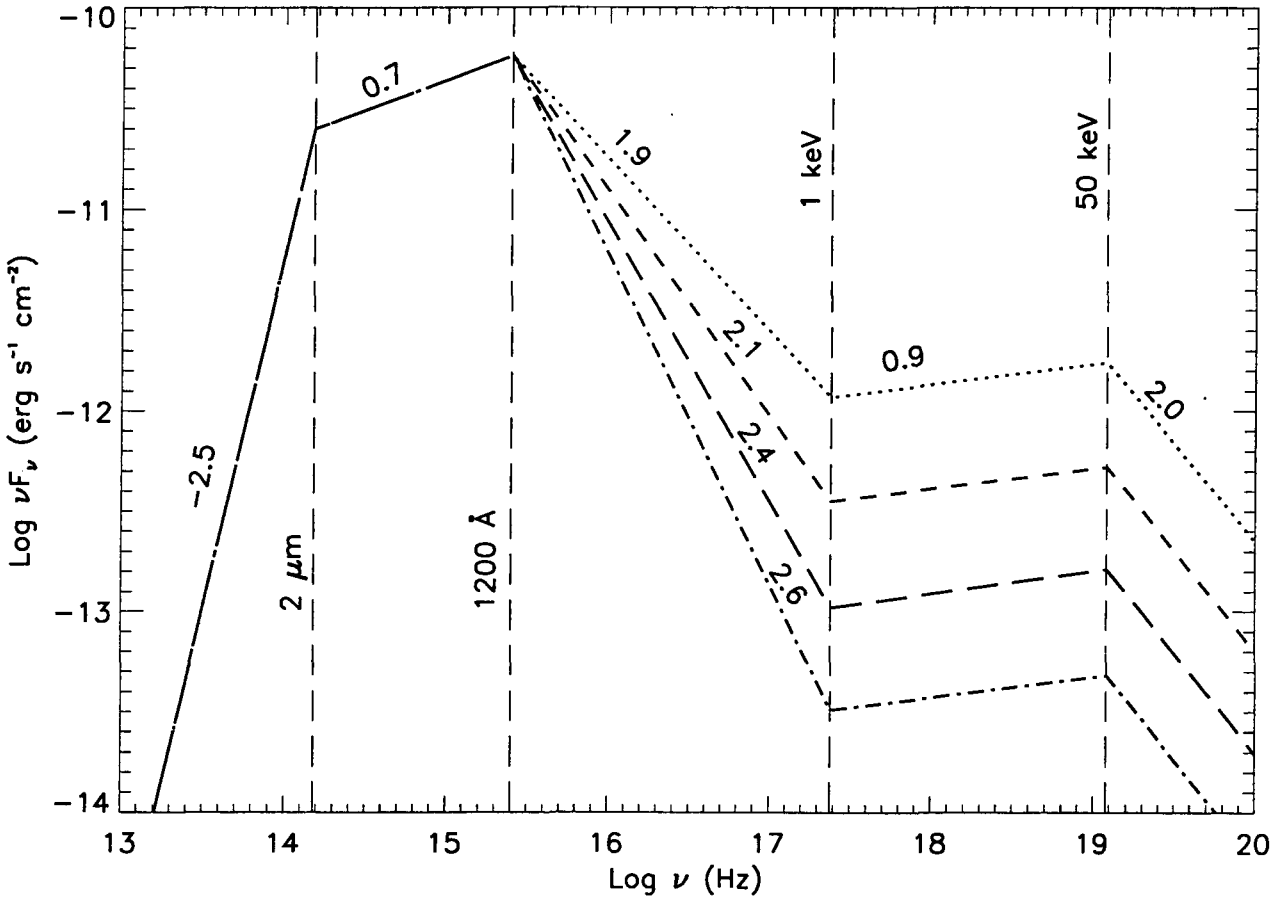

FIG. 1.— Incident piece-wise powerlaw continua used in generating the grid of ionized absorbers. The slopes are indicated ($f_\nu \propto \nu^{-\alpha}$). The dotted, dashed, long-dashed, and dash dotted lines correspond to $\alpha_{ox} = 1.6, 1.8, 2.0$, and 2.2, respectively.

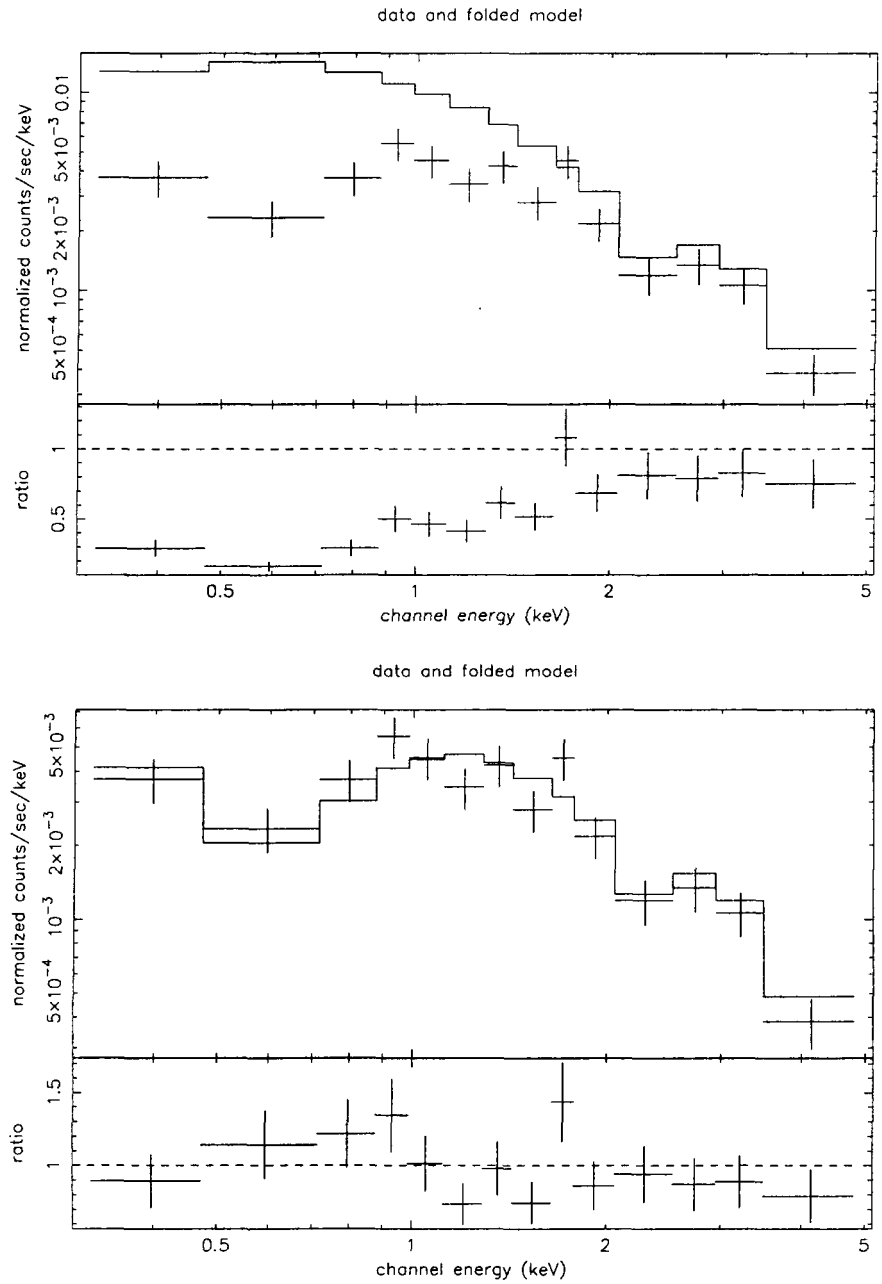

FIG. 2.— X-ray spectrum of PG 2302+029. Upper Panel: with no intrinsic absorption. Lower Panel: ionized absorber at $z \approx 0.7$. In both cases $\alpha_{ox} = 2.0$

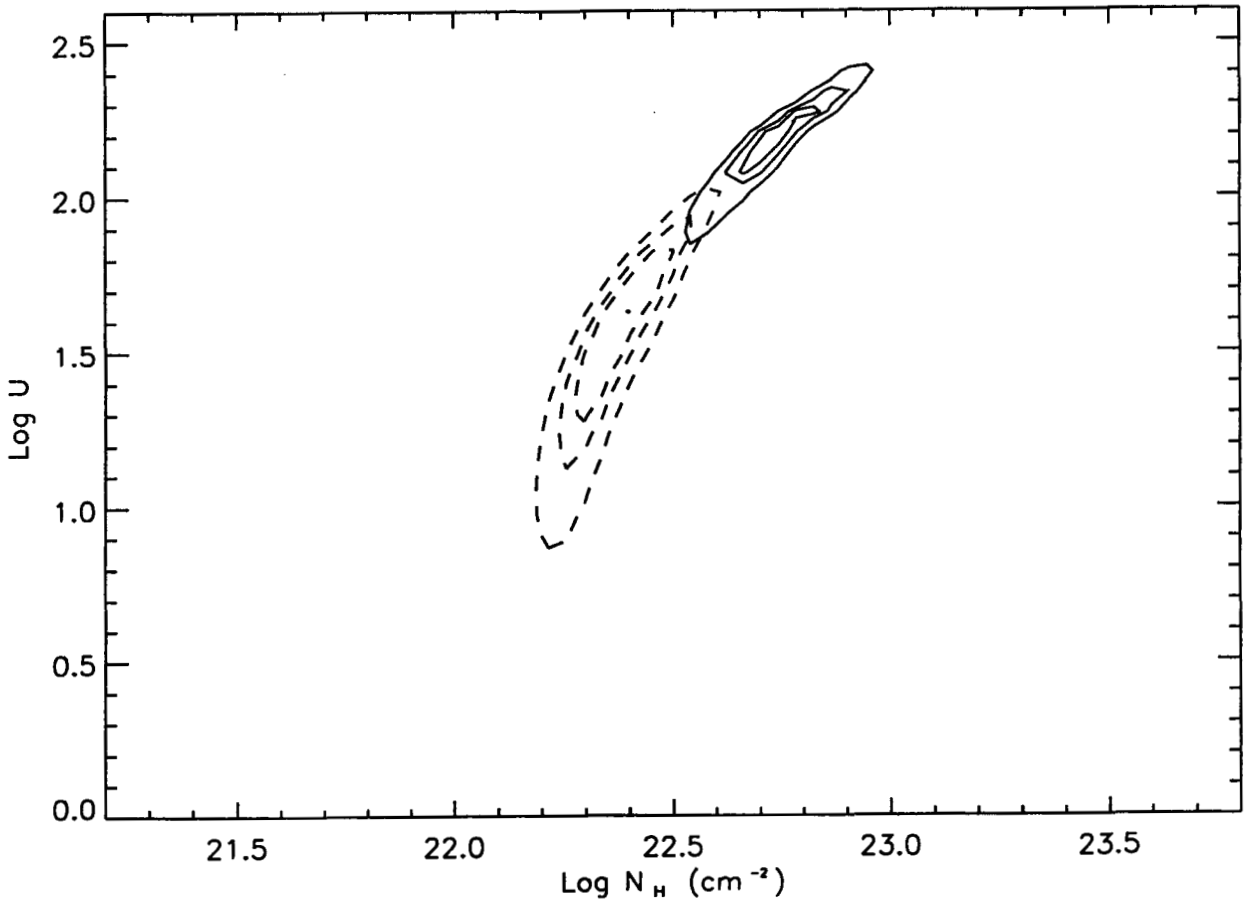

FIG. 3.— Confidence contours, 67%, 90%, and 99%, levels for X-ray fits. Solid-line contours are for $z_{Xabs} = z_{QSO}$, while dashed-line ones are for $z_{XAbs} = z_{UVabs}$.

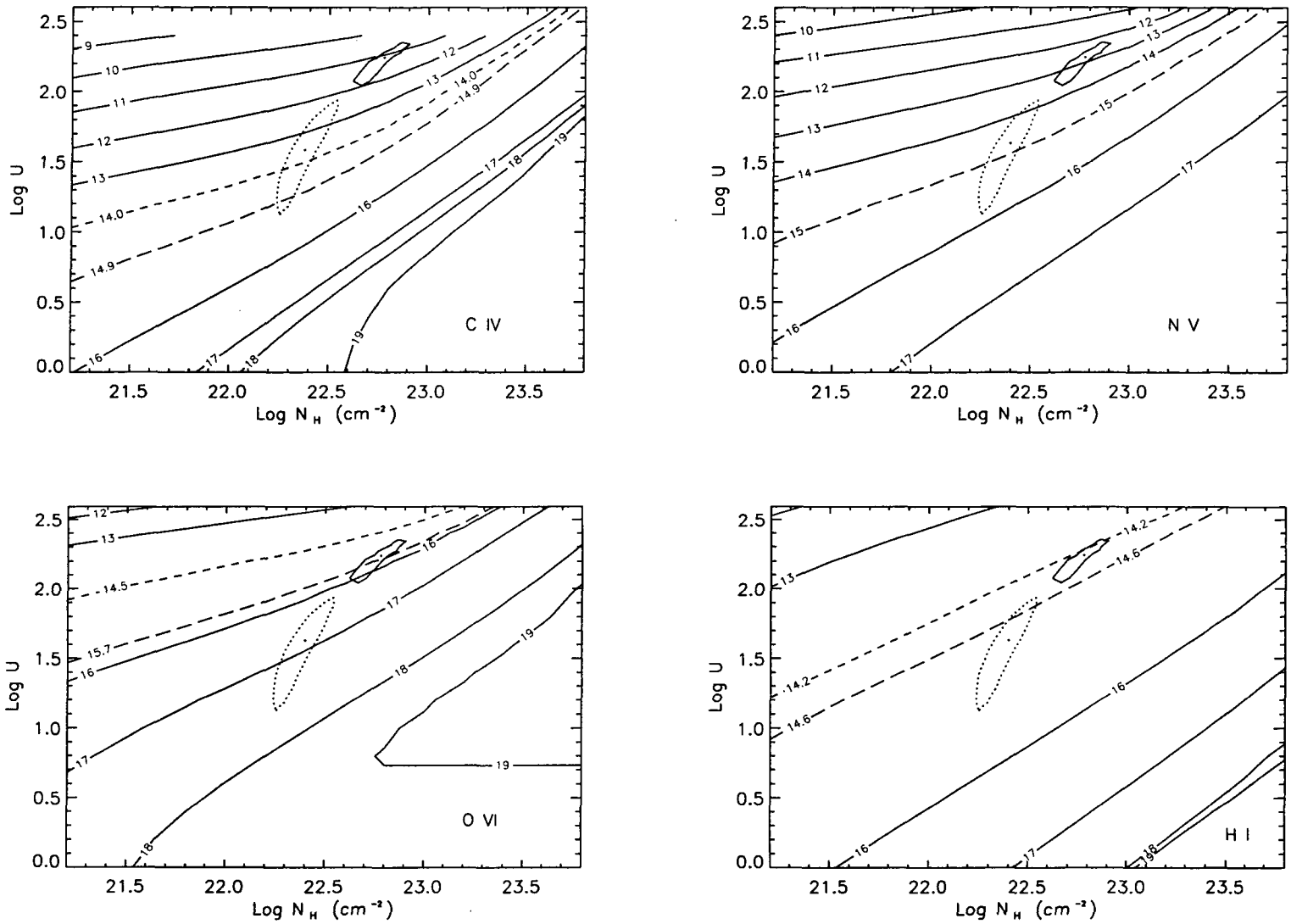

FIG. 4.— Ionic column density contours as a function of ionization parameter and total hydrogen column density. Contours are labelled by the logarithm of column density expressed in cm^{-2}, for the indicated species. Closed contours (solid: $z_{Xabs} = z_{QSO}$, dotted: $z_{XAbs} = z_{UVabs}$) are the 90% confidence levels determined from the fits to the X-ray data. The solid lines are generated from photoionization calculations. The long-dashed and short-dashed lines are the column densities measured from the FOS spectra for the broad and narrow absorption lines, respectively. The long-dashed contour for H I is an upper limit on broad Lyα absorption assuming complete line-of-sight coverage (Hamann 1997). We do not show the measurement of the narrow N V lines, since the line ratio does not make sense physically.

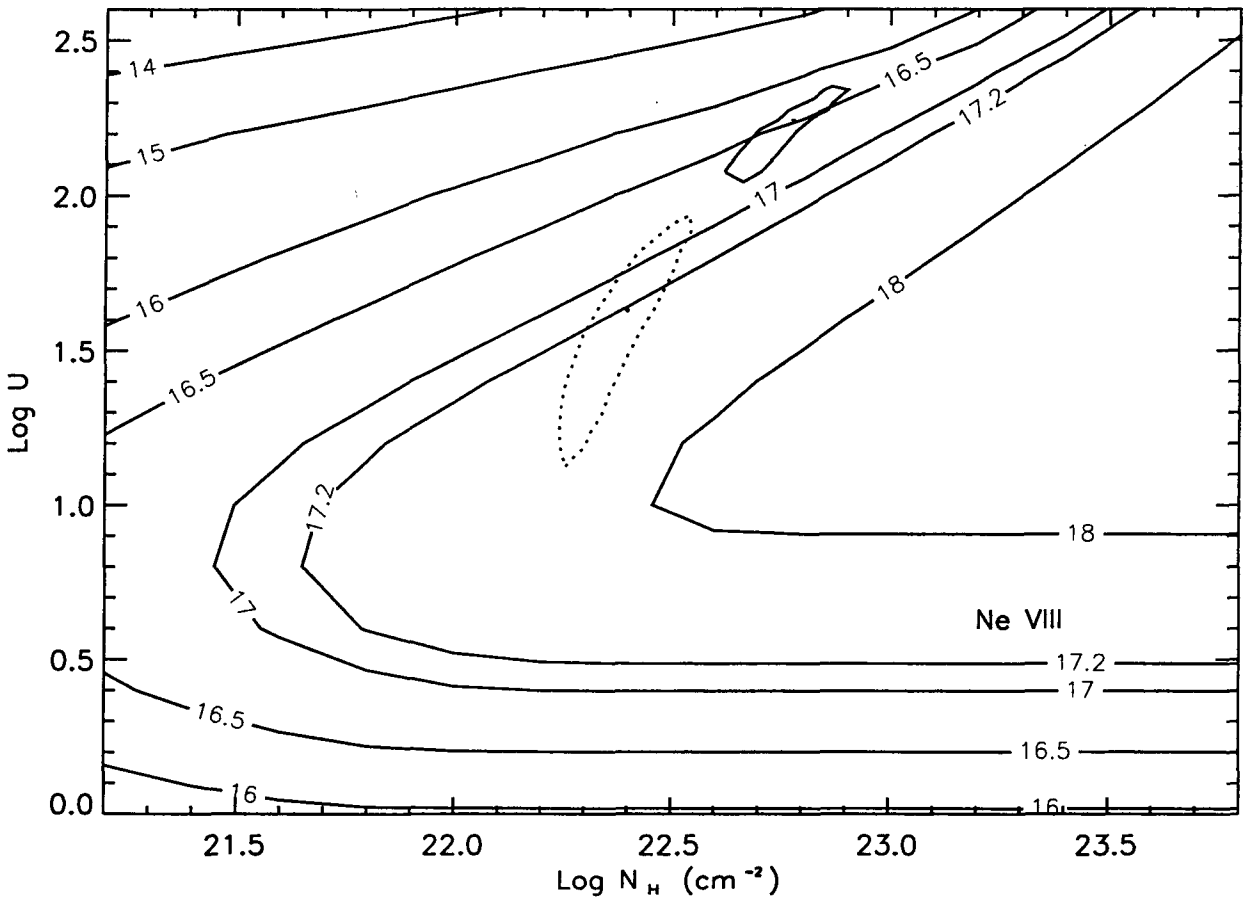

FIG. 5.— Column density contours of Ne VIII, as calculated with CLOUDY. Contour conventions are the same as in Figure 4.

DRAFT VERSION FEBRUARY 3, 2003
Preprint typeset using LaTeX style emulateapj v. 04/03/99

TABLE 1: ADOPTED UV ABSORBER PARAMETERS

From FOS Observations of 1994				
Ion	Wavelength (Å)[1]	b (km s^{-1})	W (Å)[1]	N_{ion} (cm^{-2})
C IV	1548 + 1551	2060	4.24	$10^{14.9}$
O VI	1032 + 1038	2146	7.08	$10^{15.7}$
N V	1239 + 1243	1854	3.10	$10^{15.0}$
C IV	1548	200	0.31	$10^{14.0}$
O VI	1031	330	0.37	$10^{14.5}$
H I	1216	150	0.63	$10^{14.2}$
From STIS Observations of 1998				
Ion	Wavelength (Å)[1]	b (km s^{-1})	W (Å)[1]	N_{ion} (cm^{-2})
C IV	1548 + 1551	2080	3.40	$10^{14.8}$
C IV	1548	200[2]	0.30	$10^{14.0}$

[1] Rest frame
[2] In the STIS spectrum this line is unresolved. We assumed its profile and then assumed that the b parameter matched the value measured in the earlier FOS spectrum.